MULTISCALE THREE-DIMENSIONAL STEADY SOLUTIONS IN RAYLEIGH–BÉNARD CONVECTION

Shingo Motoki, Genta Kawahara and Masaki Shimizu
Graduate School of Engineering Science
Osaka University
1-3 Machikaneyama, Toyonaka, Osaka 560-8531, Japan
motoki@me.es.osaka-u.ac.jp

ABSTRACT

Nonlinear three-dimensional steady solutions to the Boussinesq equations have been discovered for Rayleigh–Bénard convection in three-dimensional periodic domains between horizontal plates of constant temperature difference. For the Prandtl number $Pr = 1$, an unstable three-dimensional steady solution, which bifurcates from a thermal conductive state at the Rayleigh number $Ra \sim 10^3$, has been tracked up to $Ra \sim 10^7$ by using a Newton–Krylov iteration. At large Ra, the steady solution exhibits small-scale thermal plume structures near the walls with large-scale convection cells, and the Nusselt number Nu which scales with Ra as $Nu \sim Ra^{0.31}$, quite similar to the flow and thermal structures and the scaling law observed in turbulent convection. The solution also reproduces the mean temperature profiles and the root-mean-square in the velocity and temperature fluctuations of the turbulent state. The hierarchy of the vortical structures has been observed by employing the coarse graining with a Gaussian low-pass filter. The largest-scale structures correspond to the large-scale convection cells with the channel width H, whereas the smallest-scale structures are the near-wall vortical structures with approximately twice the thermal boundary layer thickness δ_θ. The scale ratio is $H/(2\delta_\theta) \approx 16$ at $Ra \sim 10^7$. In the bulk region away from the wall, the energy transfer in the wavenumber space has been discussed. In the intermediate-scale range, the kinetic energy is transferred from the large scale to the small scale, while maintaining the constant energy flux Π, which is comparable with the energy dissipation rate ε, and the energy spectral function E exhibits the Kolmogorov's $-5/3$ power law, $E \approx 1.5\varepsilon^{2/3}k^{-5/3}$.

Introduction

Rayleigh–Bénard convection is the buoyancy-driven flow between the horizontal plates heated from below, and it is one of the most canonical flows widely observed in engineering applications and nature. The effect of the buoyancy on the flow is characterized by the Rayleigh number Ra. When Ra exceeds a certain critical value Ra_c, a thermal conductive state becomes unstable to infinitesimal perturbations, and two-dimensional steady convection rolls appear (Drazin & Reid, 1981). At higher Ra, the convection becomes time-periodic, and subsequently exhibits turbulent states with multiscale thermal and vortical structures. One of the primary interests in the Rayleigh–Bénard problem is how the turbulent heat transfer scales with the Rayleigh number, that is, the dependence of the Nusselt number Nu on Ra. Over half a century ago, Malkus derived a scaling $Nu \sim Ra^{1/3}$ (Malkus, 1954) by a marginal stability argument, based on the assumption that the thermal boundary layers adapt their thickness δ_θ as $\delta_\theta/H \approx (Ra/Ra_c)^{-1/3}$, where H is the height of the fluid layer, so that the local Rayleigh number in the boundary layer becomes marginally stable. Subsequently, Kraichnan predicted a transition of the boundary layer from laminar to turbulent state, and derived the asymptotic scaling $Nu \sim Ra^{1/2}$ with logarithmic correction for very high Ra (Kraichnan, 1962), based on the mixing-length theory. The scaling $Nu \sim Ra^{1/2}$ is currently known as the 'ultimate' scaling, and obtained as the rigorous upper bound on the Nusselt number Nu by variational method (Doering & Constantin, 1996; Plasting & Kerswell, 2003). In conventional turbulent Rayleigh–Bénard convection, however, the ultimate scaling has not been observed yet. A prominent experiment by Niemela *et al.* (2000) for very high Ra exhibits $Nu \sim Ra^{0.31}$ even at $Ra \sim 10^{17}$. Recently, Grossmann and Lohse have proposed the scaling theory (Grossmann & Lohse, 2000) of global properties for Ra and the Prandtl number Pr, based on decomposing the total scalar and energy dissipation into contributions from the bulk region away from the walls and the boundary layer near the walls. A lot of experiments and numerical simulations have demonstrated the validity of the theory (Ahlers *et al.*, 2009; Stevens *et al.*, 2013). In the theory, the scaling $Nu \sim Ra^{1/3}$ is derived in the high Ra range $10^8 \lesssim Ra \lesssim 10^{14}$ for $Pr \sim 1$, and the transition to the ultimate scaling is also predicted for $Ra \gtrsim 10^{14}$. For the ultimate scaling, however, they have estimated that the effective scaling is approximately $Nu \sim Ra^{0.38}$ due to logarithmic corrections. Although some experimental results have shown the transition to $Nu \sim Ra^{0.38}$ (Chillà & Schumacher, 2012), the high-Ra scaling is still being discussed. For $10^8 \lesssim Ra \lesssim 10^{11}$, on the other hand, a lot of experimental and numerical data exhibit $Nu \sim Ra^{0.31}$ (see, e.g. He *et al.*, 2012), close to the classical scaling $Nu \sim Ra^{1/3}$.

Recently, intriguing results in two-dimensional Rayleigh–Bénard convection have been reported by Waleffe *et al.* (Waleffe *et al.*, 2015; Sondak *et al.*, 2015). They have found the scaling $Nu \approx 0.115Ra^{0.31}$, quite similar to the three-dimensional turbulent data fit $Nu \approx 0.105Ra^{0.312}$ (He *et al.*, 2012), in steady convection for high Ra range $10^7 \lesssim Ra \lesssim 10^9$. In their work, optimal two-dimensional steady solutions have been obtained so as to maximize

Nu by changing the horizontal period of the solutions. The scaling $Nu \sim Ra^{0.31}$ is achieved by a family of two-dimensional steady solutions with the horizontal period which decreases with increasing Ra. Although the result suggests that quite simple coherent structures can capture the essence of the turbulent convection, it also implies that any single two-dimensional steady solution with the fixed horizontal period (fixed maximal wavelength) cannot do it.

More recently, variational problems (Hassanzadeh *et al.*, 2014; Tobasco & Doering, 2017) to find a divergence-free velocity field optimizing scalar transport have been discussed. Motoki *et al.* (2018*a,b*) have found three-dimensional steady velocity fields as optimal states which maximize heat transfer between two parallel plates of a constant temperature difference under the constraint of fixed total enstrophy. For the large total enstrophy, the optimal states consist of convection with hierarchical self-similar vortical structures, and exhibit the scaling which corresponds to the ultimate scaling $Nu \sim Ra^{1/2}$. It should be noted that the three-dimensionality of velocity fields leads to hierarchical multiscale structures, enhancing heat transfer, in the variational problems. In the Rayleigh–Bénard convection with a horizontally periodic square domain, a three-dimensional steady solution with convection cells also bifurcates from a conductive solution at the same critical Ra as a two-dimensional steady solution (see the upper-left inset in figure 1), since the convection rolls in any horizontal direction can exist simultaneously. The three-dimensional steady solution is already unstable at its onset and so does not appear in transition to turbulence, but the unstable solution can exist until the high Rayleigh number $Ra \sim 10^7$. In this paper, we report that the three-dimensional steady solution at high Ra consists of hierarchical multiscale structures, and exhibits several important turbulence statistics.

Governing equations

Let us consider the fluid layer between two horizontal plates heated from below and cooled from above, and suppose the Boussinesq approximation, in which the fluid is incompressible and the density variation is taken into account just for the buoyancy term. The time evolution of velocity field $\boldsymbol{u}(\boldsymbol{x},t) = u\boldsymbol{e}_x + v\boldsymbol{e}_y + w\boldsymbol{e}_z$ and temperature field $T(\boldsymbol{x},t)$ are described by the Boussinesq equations

$$\nabla \cdot \boldsymbol{u} = 0, \tag{1}$$

$$\frac{\partial \boldsymbol{u}}{\partial t} + (\boldsymbol{u} \cdot \nabla)\boldsymbol{u} = -\frac{1}{\rho}\nabla p + \nu\nabla^2\boldsymbol{u} + g\alpha T\boldsymbol{e}_z, \tag{2}$$

$$\frac{\partial T}{\partial t} + (\boldsymbol{u} \cdot \nabla)T = \kappa\nabla^2 T, \tag{3}$$

where $p(\boldsymbol{x},t)$ is pressure, and ρ, ν, g, α and κ are a mass density, a kinematic viscosity, an acceleration due to gravity, a volumetric thermal expansivity and a thermal diffusivity, respectively. $\boldsymbol{e}_x$ and $\boldsymbol{e}_y$ are mutually orthogonal unit vectors in the horizontal directions while $\boldsymbol{e}_z$ is a unit vector in the vertical direction. The two horizontal plates are positioned at $z = 0$ and $z = H$, and the flow is periodic in the x- and y-directions with periods, L_x and L_y. The top (or bottom) wall surface is no-slip and impermeable, and held at lower (or higher) constant temperature $T = 0$ (or $T = \Delta T > 0$). The thermal convection is characterized by two dimensionless parameters, the Rayleigh number Ra and
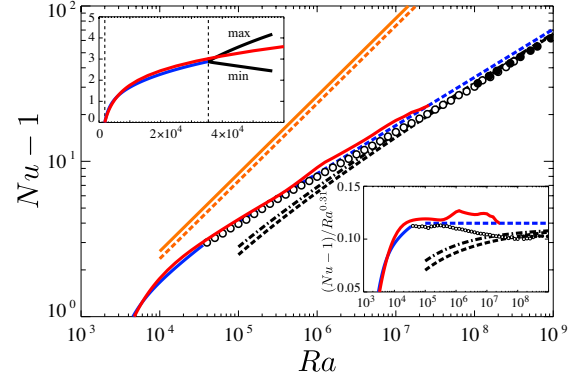
Figure 1. Nusselt number Nu as a function of Rayleigh number Ra. The red and blue solid lines respectively represent the three-dimensional and two-dimensional steady solutions bifurcating from the thermal conductive state at $Ra \approx 1879$. The open circles exhibit the present turbulent data obtained in the horizontally-square periodic domain, and the filled circles show experimental turbulent data (Niemela & Sreenivasan, 2006) in cylindrical containers. The black dashed and chain lines denote turbulent data fits $Nu = 0.088Ra^{0.32}$ (Niemela & Sreenivasan, 2006) and $Nu = 0.105Ra^{0.312}$ (He *et al.*, 2012), respectively. The blue dashed line indicates the scaling $Nu - 1 = 0.115Ra^{0.31}$ (Waleffe *et al.*, 2015; Sondak *et al.*, 2015) achieved by a family of two-dimensional steady solutions with an optimal aspect ratios so as to maximize Nu. The orange solid and dashed lines respectively indicate the best upper bound $Nu - 1 = 0.02634Ra^{1/2}$ (Plasting & Kerswell, 2003) and the scaling $Nu - 1 = 0.0236Ra^{1/2}$ (Motoki *et al.*, 2018*a*) evaluated from the optimal scaling in the variational problem to maximize heat transfer. The black solid lines in the upper-left inset show the maximal and minimum value of Nu in the three-dimensional time-periodic solution bifurcating from the two-dimensional steady solution at $Ra = 3.55 \times 10^4$. The lower-right inset shows the compensated Nu.

the Prandtl number Pr given by

$$Ra = \frac{g\alpha\Delta T H^3}{\nu\kappa}, \quad Pr = \frac{\nu}{\kappa}, \tag{4}$$

and the vertical convective heat transfer is quantified by the Nusselt number defined as

$$Nu = 1 + \frac{\langle wT \rangle}{\kappa\Delta T/H}, \tag{5}$$

where $\langle \cdot \rangle$ represents a volume and time average.

Numerical methods

The equations (1)–(3) are discretized by employing a spectral Galerkin method based on the Fourier series expansion in the periodic horizontal directions and an expansion in terms of the Chebyshev polynomials in the vertical direction. Aliasing errors are removed with the aid of the 2/3 rule for the Fourier transform and the 1/2 rule for the Chebyshev transform. Time advancement is carried out with the
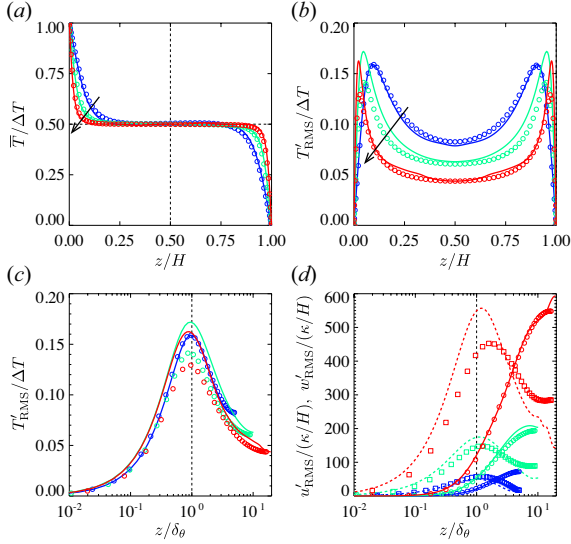
Figure 2.   Mean temperature and root-mean-square (RMS) of the temperature and velocity fluctuations as a function of (a,b) z/H and (c,d) z/δ_θ in the three-dimensional steady solution (lines) and the turbulent state (symbols). The blue, green and red plots are respectively obtained at $Ra = 10^5$, $Ra = 10^6$ and $Ra = 10^7$, and the arrows in (a,b) indicate the direction of increasing Ra. The solid lines and circles in (d) show the vertical velocity, and the dashed lines and squares are the horizontal velocity. δ_θ is the thermal boundary layer thickness scales as $\delta_\theta/H = 1/(2Nu)$.

Figure 3.   Flow and thermal structures in the three-dimensional steady solution at (a) $Ra = 10^5$, (b) $Ra = 10^6$ and (c) $Ra = 10^7$, and (d) the turbulent state at $Ra = 10^7$. The yellow and gray objects respectively represent the iso-surfaces of the temperature $T/\Delta T = 0.6$ and the positive second invariant of the velocity gradient tensor, (a) $Q/(\kappa^2/H^4) = 1.28 \times 10^5$, (b) $Q/(\kappa^2/H^4) = 2.4 \times 10^6$ and (c,d) $Q/(\kappa^2/H^4) = 8 \times 10^7$. The contours represent temperature field T in the plane $y/H = \pi/4(= -\pi/4)$, and the velocity vectors (u,w) are superposed in the enlarged views in (c,d). δ_θ is the thermal boundary layer thickness scales as $\delta_\theta/H = 1/(2Nu)$.

Crank–Nicholson scheme for the diffusion terms and the second-order Adams–Bashforth scheme for the nonlinear and buoyancy terms. The nonlinear steady solutions are obtained by the Newton–Krylov iteration (for details, see Sondak *et al.*, 2015; Motoki *et al.*, 2018b).

In this paper, we present steady solutions and turbulent states obtained in the horizontally-square periodic domain of $L = L_x = L_y = (\pi/2)H$ for $Pr = 1$. For the domain size $L = (2\pi/\alpha_c)H$, where $\alpha_c = 3.117$ is the critical wavenumber corresponding to the minimal critical $Ra = 1708$ in the linear stability analysis (Drazin & Reid, 1981), we have confirmed that the effects of the domain size are insignificant on the scaling of Nu with Ra for large Ra as well as the flow and thermal structures in the three-dimensional steady solutions, which will be discussed in the following sections. In addition, for $Pr = 7$, we have obtained similar results. The numerical computations are carried out on 128^3 grid points for $Ra < 10^7$ and 256^3 grid points for $Ra \geq 10^7$. It has been validated in comparison between the two resolutions that the results presented in this paper are independent of the spatial resolution at $Ra \sim 10^7$.

Nu-Ra scaling

Steady solutions, which bifurcate from a conductive state at $Ra \sim 10^3$, has been obtained up to $Ra \sim 10^7$ (figure 1). The red line shows a three-dimensional steady solution, and it exhibits the scaling $Nu \sim Ra^{0.31}$ at $Ra \gtrsim 10^5$, corresponding to the scaling, $Nu \approx 0.088Ra^{0.32}$ (Niemela & Sreenivasan, 2006) (black dashed) and $Nu \approx 0.105Ra^{0.312}$ (He *et al.*, 2012) (chain), observed in large-Rayleigh-number turbulent convections for $Ra \lesssim 10^{11}$. The open and filled circles respectively represent the present turbulent data in the horizontally-square periodic domain and

the experimental data obtained in a cylindrical container (Niemela & Sreenivasan, 2006). The heat flux of the three-dimensional steady solution is only slightly larger than that of the turbulent states, and it is quite similar to the optimal heat flux $Nu - 1 \approx 0.115Ra^{0.31}$ (Waleffe *et al.*, 2015; Sondak *et al.*, 2015) (blue dashed) achieved by a family of two-dimensional steady solutions with optimal horizontal periods so as to maximize Nu.

The orange dashed line indicates an optimal scaling $Nu - 1 \approx 0.0236Ra^{1/2}$ (Motoki *et al.*, 2018a), corresponding to the rigorous upper bound $Nu - 1 \approx 0.02634Ra^{1/2}$ (Plasting & Kerswell, 2003) (orange solid) and the asymptotic ultimate scaling in the Rayleigh–Bénard convection. The optimal scaling is achieved by the three-dimensional optimal states in the variational problem of maximizing heat transfer under the constraint of fixed total enstrophy. The optimal solutions require external body force which is different from buoyant force, since the optimization does not necessarily require that the velocity fields obey particular physical equations of motion, e.g., the Boussinesq equation. However, the three-dimensional optimal solutions are continuously connected to the present three-dimensional steady solution to the Boussinesq equation, via homotopy from the body force to the buoyancy.

The three-dimensional steady solution reproduces the mean temperature of convective turbulence in the whole

region and furthermore the RMS values are also in good agreement with each other (figure 2). $\overline{(\cdot)}$ represents the horizontal and time average, and $(\cdot)'$ denotes the fluctuation about the horizontal average for the steady solutions and the horizontal and time average for the turbulent states. In the bulk region, all the mean temperature profiles are flattened as a result of almost complete mixing by large-scale convection. Unstable stratification is significant only in the near-wall region. The thermal boundary layer thickness δ_θ scales as

$$\delta_\theta/H = 1/(2Nu) \sim Ra^{-0.31}, \tag{6}$$

in accord with the marginally stable argument by Malkus (Malkus, 1954). As shown in figures 2(c,d), the positions of the maximal peaks of T'_{RMS} and u'_{RMS} scale as $z/\delta_\theta \approx 1$.

Flow and thermal structures

Figure 3 visualizes spatial flow and thermal structures in the three-dimensional steady solution and the turbulent state at $Ra = 10^5, 10^6$ and 10^7. The yellow objects show isosurfaces of the temperature $T/\Delta T = 0.6$, representing high-temperature plumes, and the gray objects display vortex structures visualized by the positive second invariant of the velocity gradient tensor, $Q = -(\partial u_i/\partial x_j)(\partial u_j/\partial x_i)/2$. The three-dimensional steady solution consists of large-scale convection cells and small-scale vortex structures. As Ra increases, smaller plume structures (and relevant smaller and stronger tube-like vortex structures) appear near the walls while maintaining large-scale structures. It should be stressed that the single three-dimensional steady solution spontaneously reproduces multiscale structures. In two-dimensional steady convection (Waleffe *et al.*, 2015), the appearance of such smaller-scale plume (and vortex) structures has not been observed for a fixed horizontal period, and the scaling $Nu \sim Ra^{0.31}$ is achieved by a family of solutions with the smaller horizontal periods with increasing Ra.

At $Ra = 10^7$ (figure 3c), near the wall, we can observe the sheet-like thermal plumes with the smallest-scale tube-like vortices visualized by the positive second invariant, which are quite similar to those observed in the snapshot of the turbulent state (figure 3d). The smallest-scale structures are generated in the unstable stratification near the wall, and the size of the plumes and vortices scale with the thermal boundary layer thickness δ_θ.

Hierarchical vortex structures

Developed turbulence organizes hierarchical coherent vortical structures with various scales (Goto *et al.*, 2017; Motoori & Goto, 2019). As shown in figure 3, we can extract smallest-scale vortical structures by employing the isosurfaces of Q. However, it is difficult to find out large- and intermediate-scale coherent structures. To examine a hierarchy in the three-dimensional steady solution, we consider coarse graining the velocity field $\boldsymbol{u}(\boldsymbol{x})$. The coarse-grained velocity field $\boldsymbol{u}^*(\boldsymbol{x})$ is obtained by the Gaussian low-pass filter (Lozano-Durán *et al.*, 2016; Motoori & Goto, 2019) as

$$\boldsymbol{u}^*(\boldsymbol{x}) = \int_V a \cdot \boldsymbol{u}(\boldsymbol{x}') \exp\left\{-\left(\frac{\pi\Delta r}{\sigma}\right)^2\right\} d\boldsymbol{x}', \tag{7}$$
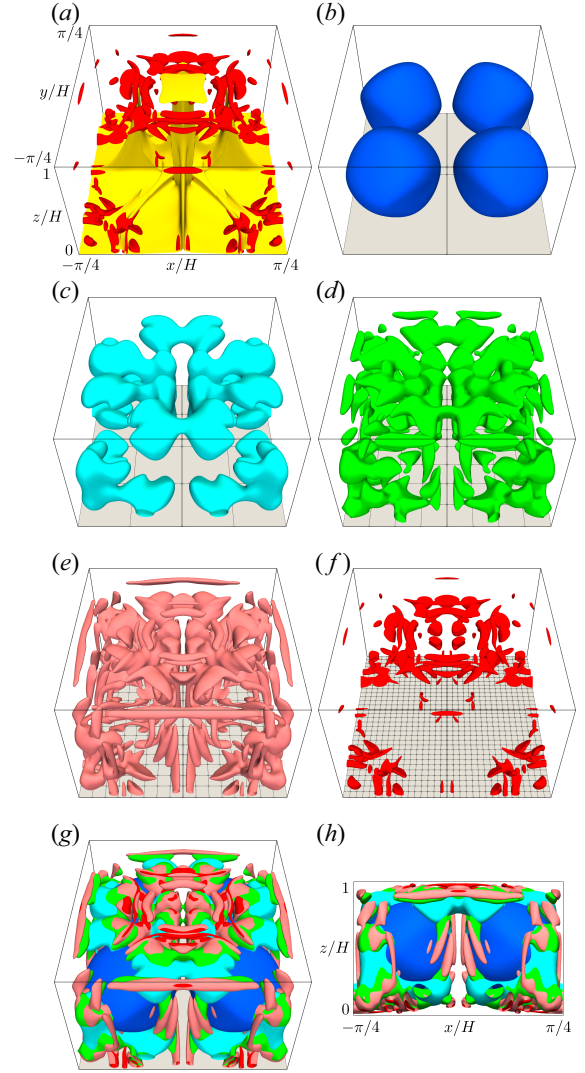
Figure 4. Hierarchical vortical structures in the three-dimensional steady solution at $Ra = 2.6 \times 10^7$, which are visualized by the coarse graining with the Gaussian low-pass filter. (a) Non-filtered velocity and temperature fields. The red and yellow objects show the isosurfaces of the second invariant of the velocity gradient tensor, $Q/(\kappa^2/H^4) = 2 \times 10^8$, and the temperature $T/\Delta T = 0.6$, respectively. (b-h) Filtered velocity fields with the various filter widths. The vortical structures are visualized by the isosurfaces of $Q/(\kappa^2/H^4)$ of the filtered velocity fields with the filter width $\sigma = H(= 2L/\pi)$ (blue), $\sigma = L/4$ (light blue), $\sigma = L/8$ (green), $\sigma = L/16$ (light red), $\sigma = L/32$ (red), and they are superposed in (g,h). The isosurface levels are (blue) 5×10^5, (light blue) 4×10^6, (green) 1.2×10^7, (light red) 3×10^7, (red) 1.6×10^8.

where $\Delta r = \sqrt{(x'-x)^2 + (y'-y)^2 + (z'-z)^2}$, σ is the filter width and a is constant such that the integral of the kernel over the control volume V is unity. In the wall-normal direction, the Gaussian filter is applied by employing the method of reflecting it at the wall, proposed by Lozano-Durán *et al.* (2016).

Figure 4 shows hierarchical vortical structures which are found out in the three-dimensional steady solution at $Ra = 2.6 \times 10^7$. Non-filtered velocity and temperature fields are shown in figure 4(a), and isosurfaces of the positive
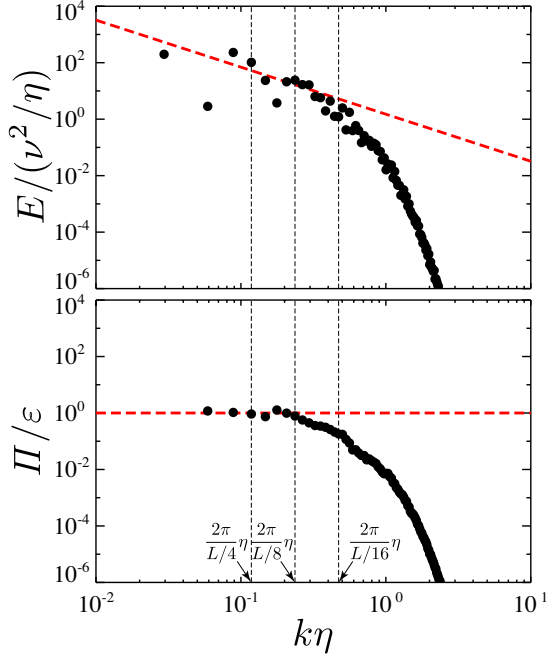
Figure 5.   (*a*) Energy spectra $E(k,z)$ and (*b*) energy flux $\Pi(k,z)$, at the center of the fluid layer, $z = H/2$, in the three-dimensional steady solution at $Ra = 2.6 \times 10^7$. The lateral and longitudinal axes are normalized by the Kolmogorov micro-scale length $\eta(z) = (\nu^3/\varepsilon(z))^{1/4}$ and the energy dissipation rate at each hight, $\varepsilon(z) = \nu\overline{|\nabla \boldsymbol{u}|^2}$. The red dashed lines in (*a*) and (*b*) indicate $E = 1.5\varepsilon^{2/3}k^{-5/3}$ and $\Pi/\varepsilon = 1$, respectively.

Energy transfer in wavenumber space

In the three-dimensional steady solution at large *Ra*, as can be seen in figures 4(*d,e*), the intermediate-scale vortical structures exist in the bulk region as well as the near-wall regions. Figures 4(*g,h*) show the superposed structures, and from their spatial distribution it is conjectured that the bulk flow is composed of the multiscale coherent structures.

Figure 5(*a*) shows the energy spectral function $E(k,z)$,

at the center of the fluid layer, $z = H/2$, defined as

$$E(k,z) = \frac{L}{2\pi} \sum_{k-\frac{\Delta k}{2} < |\boldsymbol{k}_{2D}| < k+\frac{\Delta k}{2}} \frac{1}{2}|\widetilde{u}(\boldsymbol{k}_{2D},z)|^2, \quad (8)$$

where $\widetilde{(\cdot)}$ indicates the Fourier coefficients only in the periodic horizontal (*x*- and *y*-) directions. $\boldsymbol{k}_{2D} = (k_x, k_y)$ and $k = \sqrt{k_x^2 + k_y^2}$ are respectively the wavenumber vector and its magnitude, and $\Delta k = 2\pi/L$. The lateral and longitudinal axes are normalized by the Kolmogorov micro-scale $\eta(z) = (\nu^3/\varepsilon)^{1/4}$, which is based on the energy dissipation rate at each hight, $\varepsilon(z) = \nu\overline{|\nabla \boldsymbol{u}|^2}$. In the wavenumber band $2\pi/(L/4) \lesssim k\eta \lesssim 2\pi/(L/16)$, corresponding to the intermediate-scale range, we can find that the energy spectra exhibit the well-known Kolmogorov's $-5/3$ power law, $E = C_K\varepsilon^{2/3}k^{-5/3}$ (Kolmogorov, 1941), with the constant $C_K \approx 1.5$ which is comparable with the Kolmogorov constant in the inertial subrange of high-Reynolds-number turbulence (Sreenivasan, 1995).

We here consider the energy flux in the wavenumber space, $\Pi(k,z)$ (Mizuno, 2016), defined as

$$\Pi(k,z) = \sum_{k' \geq k} \sum_{k-\frac{\Delta k}{2} < |\boldsymbol{k}_{2D}| < k+\frac{\Delta k}{2}} T^s(\boldsymbol{k}_{2D},z), \quad (9)$$

$$T^s(\boldsymbol{k}_{2D},z) = \Re\left[\partial_j\widetilde{u}_i(\widetilde{u_i\widetilde{u}_j})^\dagger - \frac{1}{2}\frac{\mathrm{d}\widetilde{u}_j(\widetilde{u_j\widetilde{w}})^\dagger}{\mathrm{d}z}\right], \quad (10)$$

where $(\partial_1, \partial_2, \partial_3) = (ik_x, ik_y, \partial/\partial z)$ and $\dagger$ denotes the complex conjugate. $T^s(\boldsymbol{k}_{2D},z)$ represents the energy transfer between the Fourier modes, and the sum of all the spectral components does not contribute to the total energy budget, i.e., $\sum_{\boldsymbol{k}_{2D}} T^s(\boldsymbol{k}_{2D},z) = 0$. The energy flux in the three-dimensional steady solution is shown in figure 5(*b*). In the intermediate-scale range, the energy flux represents a positive value scales with the same order of the energy dissipation rate ε, in accord with the the Kolmogorov-Obukhov energy cascade view that the energy flux in inertial subrange remains constant, and balances with the energy dissipation rate. It is quite intriguing that such a time-independent solution exhibits the energy transfer from large to small scale in the wavenumber space, in common with developed turbulence.

Acknowledgements

REFERENCES

Ahlers, G., Grossmann, S. & Lohse, D. 2009 Heat transfer and large scale dynamics in turbulent Rayleigh–Bénard convection. *Rev. Mod. Phys.* **81**, 503–537.

Chillà, F. & Schumacher, J. 2012 New perspectives in turbulent Rayleigh–Bénard convection. *Eur. Phys. J.* E **35** (58).

Doering, C. R. & Constantin, P. 1996 Variational bounds on energy dissipation in incompressible flows. III. Convection. *Phys. Rev.* E **53** (6), 5957–5981.

values of Q of the filtered velocity field $\boldsymbol{u}^*$ with the filter width $\sigma = H(= 2L/\pi), L/2, L/4, L/8$ and $L/16$ are respectively displayed in figure 4(*b-f*). The blue objects in figure 4(*b*) are largest-scale structures corresponding to the large-scale convection cells, whereas the red objects in figure 4(*f*) are smallest-scale vortical structures with the size of $\sigma/2 = L/32 \approx 2\delta_\theta$, which coincide with the vortices observed in the non-filtered velocity field (figure 4*a*). The light blue, green and light red objects in figures 4(*c,d,e*) display intermediate-scale vortical structures with the eight, four and two times the size of the smallest-scale vortices, respectively. We can see that the smaller-scale vortical structures exist closer to the wall. For the variational problem (Motoki *et al.*, 2018*a*), similar hierarchal structures can be found in the three-dimensional steady optimal states. In the velocity field optimized within a two-dimensional field, on the other hand, such multiscale structures have not been observed (Hassanzadeh *et al.*, 2014).

Drazin, P. G. & Reid, W. H. 1981 Hydrodynamic stability. *Cambridge University Press* .

Goto, S., Saito, Y. & Kawahara, G. 2017 Hierarchy of antiparallel vortex tubes in spatially periodic turbulence at high reynolds numbers. *Phys. Rev. Fluids* **2** (064603).

Grossmann, S. & Lohse, D. 2000 Scaling in thermal convection: a unifying theory. *J. Fluid Mech.* **407**, 27–56.

Hassanzadeh, P., Chini, G. P. & Doering, C. R. 2014 Wall to wall optimal transport. *J. Fluid Mech.* **751**, 627–662.

He, X., Funfschilling, D., Nobach, H., Bodenschatz, E. & Ahlers, G. 2012 Transition to the ultimate state of turbulent Rayleigh–Bénard convection. *Phys. Rev. Lett.* **108** (024502).

Kolmogorov, A. N. 1941 The local structure of turbulence in incompressible viscous fluid for very large reynolds numbers. *Dokl. Akad. Nauk SSSR* **30**, 301–305.

Kraichnan, R. H. 1962 Turbulent thermal convection at arbitrary Prandtl number. *Phys. Fluids* **5** (1374).

Lozano-Durán, A., Holzner, M. & Jimenez, J. 2016 Multiscale analysis of the topological invariants in the logarithmic region of turbulent channels at a friction reynolds number of 932. *J. Fluid Mech.* **803**, 356–394.

Malkus, W. V. R. 1954 The heat transport and spectrum of thermal turbulence. *Proc. R. Soc. Lond.* A **225**, 196–212.

Mizuno, Y. 2016 Spectra of energy transport in turbulent channel flows for moderate reynolds numbers. *J. Fluid Mech.* **805**, 171–187.

Motoki, S., Kawahara, G. & Shimizu, M. 2018*a* Maximal heat transfer between two parallel plates. *J. Fluid Mech.* **851** (R4).

Motoki, S., Kawahara, G. & Shimizu, M. 2018*b* Optimal heat transfer enhancement in plane Couette flow. *J. Fluid Mech.* **835**, 1157–1198.

Motoori, Y. & Goto, S. 2019 Generation mechanism of a hierarchy of vortices in a turbulent boundary layer. *J. Fluid Mech.* **865**, 1085–1109.

Niemela, J. & Sreenivasan, K. R. 2006 Turbulent convection at high Rayleigh numbers and aspect ratio 4. *J. Fluid Mech.* **557**, 411–422.

Niemela, J. J., Skrbek, L., Sreenivasan, K.R. & Donnelly, R. J. 2000 Turbulent convection at very high Rayleigh numbers. *Nature* **404**, 837–840.

Plasting, S. C. & Kerswell, R. R. 2003 Improved upper bound on the energy dissipation rate in plane Couette flow: the full solution to Busse's problem and the Constantin–Doering–Hopf problem with one-dimensional background field. *J. Fluid Mech.* **477**, 363–379.

Sondak, D., Smith, L. M. & Waleffe, F. 2015 Optimal heat transport solutions for Rayleigh–Bénard convection. *J. Fluid Mech.* **784**, 565–595.

Sreenivasan 1995 On the universality of the kolmogorov constant. *Phys. Fluids* **7** (2778).

Stevens, R. J. A. M., van der Poel, E. P., Grossmann, S. & Lohse, D. 2013 The unifying theory of scaling in thermal convection: the updated prefactors. *J. Fluid Mech.* **730**, 295–308.

Tobasco, I. & Doering, C. R. 2017 Optimal wall-to-wall transport by incompressible flows. *Phys. Rev. Lett.* **118**, 264502.

Waleffe, F., Boonkasame, A. & Smith, L. M. 2015 Heat transport by coherent Rayleigh–Bénard convection. *Phys. Fluids* **27** (051702).